

Corrosion Behavior of Fe-Al Alloy Modified with Cr and Ti in Simulated Physiological Human Media.

R. A. Rodríguez-Díaz^{1,2,*}, J. Uruchurtu-Chavarín¹, A. Molina-Ocampo¹, J. Porcayo-Calderón³, M. González-Pérez², J.M. López-Oglesby², J. G. Gonzalez-Rodríguez¹ and J. A. Juárez-Islas⁴

¹ Centro de Investigación en Ingeniería y Ciencias Aplicadas, UAEM, Av. Universidad 1001, Col. Chamilpa, Cuernavaca Mor., México.

² Universidad Popular Autónoma del Estado de Puebla, A. C.; 21 sur No. 1103, Colonia Santiago, C. P. 72160 Puebla, Puebla, México.

³ I.I.E., Gerencia de Procesos Térmicos, Av. Reforma 120, Temixco, Mor., México.

⁴ Instituto de Investigaciones en Materiales-UNAM, circuito exterior S/N, Ciudad Universitaria, C. P. 04510, México DF, México.

*E-mail: rdiaz.unam@gmail.com, robertoademar.rodriguez@upaep.mx

Received: 15 November 2012 / Accepted: 6 December 2012 / Published: 1 January 2013

This paper presents an investigation on the effect of the addition of the alloying elements (Cr, and Ti) on the corrosion resistance of intermetallic alloys of iron aluminides FeAl, in an environment that simulates human body fluids. Potentiodynamic polarization curves showed that the binary alloy Fe40Al exhibited the greatest resistance to corrosion while the alloy Fe40Al2.5Cr (% at.) showed the lowest resistance to corrosion. Linear polarization resistance curves R_p , Nyquist data and Bode curves obtained by electrochemical impedance spectroscopy, suggest the development of a thick passive layer consisting mainly of Cr_2O_3 and TiO_2 , in addition to the protective oxide layer formed by oxides of Al and Fe.

Keywords: Corrosion, aluminides, intermetallic compounds, Hank's solution, electrochemical techniques.

1. INTRODUCTION

A biomaterial is a synthetic or natural material used in a medical device intended to interact with biological systems [1].

In medical science applications, biomaterials are rarely used as isolated materials but rather are integrated into devices or implants [2, 3]. The fundamental requirement for any biomaterial is that material and body tissue environment can coexist without any undesirable effects on each other. This

condition is known as biocompatibility, and is more specifically defined as the ability of a material to perform with an appropriate host response in a specific biological application [4].

Biomaterials are commonly classified into metals, ceramics, polymers, glasses, carbons, and composite materials [5].

Some examples of applications of metals and alloys used as biomaterials in medicine are: Ti [6], Ti-Al-V [7] alloys and stainless steel [8] used in joint replacements in hip, knee and dental implants, while stainless steel, and Co-Cr [9] alloys are used as a bone plate for fracture fixation.

Aluminides are receiving considerable attention due to their interesting aqueous corrosion behaviors in acidic, basic, chloride and sulfur-compound solutions.

Among the newest room temperature applications of these materials are biomaterials, implants and seawater environment applications [10– 12].

Although iron aluminides have been investigated primarily for high temperature structural applications due to its ability to form a protective layer of aluminum oxide that provides corrosion resistance in molten salt environments [13, 14], its excellent performance in these conditions has motivated further study in aqueous solutions. The use of iron aluminides is being considered for applications at room temperature to replace stainless steels in biomedical implants [15].

Thus, the purpose of this work is to investigate the effect of alloying with Cr and Ti a FeAl alloy on its corrosion resistance in simulated physiological human media for their potential application as biomaterials.

2. EXPERIMENTAL PROCEDURES

2.1 Materials

Cast ingots of binary Fe-40 at. % Al and ternary Fe₄₀Al-X (X = 2.5 at. % Cr or Ti) alloys were elaborated using a high-frequency vacuum induction furnace. High purity (99.9 %) Fe, Al, Cr and Ti were placed in a silicon carbide crucible for induction melting. The molten Fe-40Al, Fe₄₀Al-X alloys were poured into a rectangular steel mold.

2.2 Sample preparation

The produced ingots were cut by a diamond wheel cutter into small rectangular parallelepiped pieces. Specimens with an exposed area ranging from 0.5 to 1.0 cm² were prepared by encapsulation in epoxy resin. Metallographic preparation of encapsulated specimens was performed by grinding the specimens from 240 to 1500 grit paper and polished with 1 μm alumina powder.

2.3 Electrochemical techniques

In order to simulate the physiological conditions of human body, biomimetic environment corrosion testing was performed in Hank's solution. The chemical composition for this environment

for in vitro corrosion studies is given in Table 2. It was prepared with double distilled water and analytical grade reagents following previously-reported methods [19].

Electrochemical tests were performed using an ACM Instruments potentiostat controlled by a computer. All potentials were measured using a Saturated Calomel Electrode (SCE) as reference electrode and a graphite bar counter electrode. All tests were performed at 30 ± 2 °C. Electrochemical techniques included potentiodynamic polarization curves, linear polarization resistance (LPR) and electrochemical impedance spectroscopy (EIS) measurements.

Potentiodynamic polarization curves were obtained by varying the applied potential with respect to the free corrosion potential, E_{corr} , from (-500 mV) up to +500 mV at a scan rate of (1 mV/s)-

Before the experiments, E_{corr} value was measured for approximately 15 minutes, until it achieved a stable reading.

EIS tests were carried out at E_{corr} by using a signal with amplitude of 20 mV and a frequency interval of 0.05 Hz-10 kHz every 24 hours for 30 days.

Measurements of LPR were performed by polarizing the specimen from +10 to -10 mV, with respect to E_{corr} , at a scan rate of 1 mVs^{-1} during 30 days.

Microstructural characterization and surface analysis of as-cast and corroded samples was performed in a Karl Zeiss DSM-950 scanning electron microscope (SEM).

Table 1. Chemical composition of the Hank's solution.

compound	NaCl	CaCl ₂	KCl	Glucose	NaHCO ₃	MgCl ₂ .6H ₂ O	Na ₂ HPO ₄ .2H ₂ O	KH ₂ PO ₄	MgSO ₄ 7H ₂ O
g/l	8	0.14	0.4	1	0.35	1	0.06	0.06	0.06

3. RESULTS AND DISCUSSION

3.1. Microstructure of un-corroded as-cast alloys.

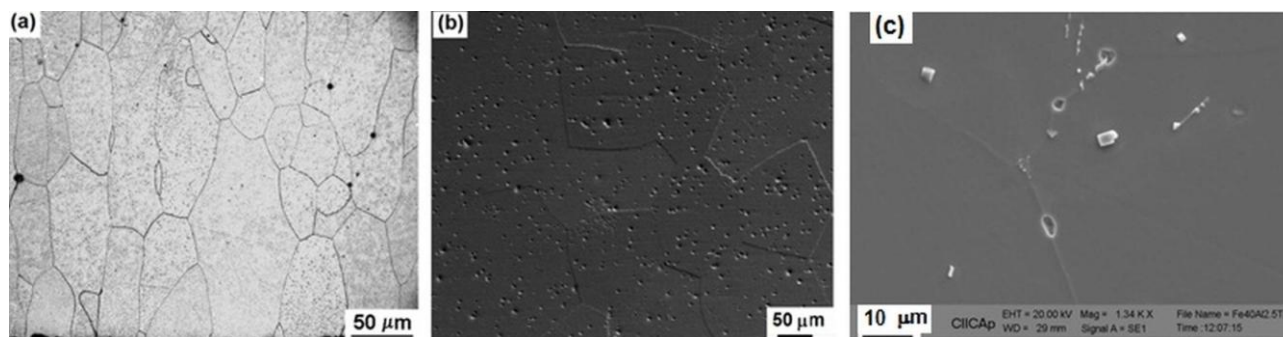


Figure 1. Microstructures of the alloys a) Fe40Al b) Fe40Al2.5Cr and c) Fe40Al2.5Ti in as-cast condition before corrosion tests.

The microstructure of the as-cast Fe40Al alloy is shown in Figure 1 a), which primarily exhibits grains with columnar morphology. Scanning electron microscopy and chemical analyses using

the EDS technique did not reveal precipitates on the surface of this alloy. This observation is consistent with the wide interval of composition (35-50 at.% Al) which contains a FeAl phase with a B2 type crystal structure according to the phase diagram of Fe-Al system [16]. This alloy presented a chill-type microstructure with three typical grain morphologies: chill, equiaxed and columnar. The mean grain size of chill morphology grains was $276 \pm 88 \mu\text{m}$, the dimensions of the columnar grains were $280 \pm 94 \mu\text{m}$ in width and $2200 \pm 130 \mu\text{m}$ in length. Grain size of equiaxed morphology was $548 \pm 91 \mu\text{m}$.

Figure 1 b) shows the microstructure of the as-cast Fe₄₀Al_{2.5}Cr alloy, which exhibits a predominantly equiaxed grain morphology with an average size of $141.2 \pm 29.3 \mu\text{m}$. No precipitates were observed in this ternary alloy, which could have formed by the addition of Cr. X-ray diffraction analysis for this alloy presented a B2 crystal structure corresponding to the FeAl alloy without the presence of second phases. These results are consistent with a previous investigation [17], which reported that the Cr element enters in solid solution in the FeAl matrix as long as the addition of this element does not exceed 5 at. %.

Fig. 1 c) shows the as-cast Fe₄₀Al_{2.5}Ti alloy, which shows the intersection of three grains with an average grain size of $150 \mu\text{m}$. Brilliant precipitates with quasi rectangular morphology are observed both the inside and the border of the grains. Pores can be observed along the grain boundaries, these sites could have been occupied by precipitates which were separated by the metallographic polishing effect. The EDS chemical analyses revealed that these precipitates constituted by Fe, Al and Ti correspond to a Fe₂TiAl phase with a L₂₁ Heusler-type crystalline structure since the region which contains Fe₂TiAl phase is just above the zone in which exists the B2 type phase in the Fe-Al-Ti system [18].

3.2 Potentiodynamic polarization curves

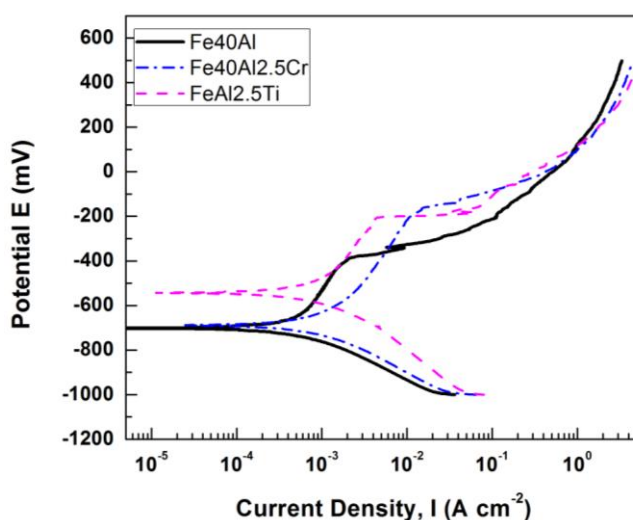


Figure 2. The effect of Cr and Ti addition on the polarization curves for Fe₄₀Al intermetallic alloys in Hank's solution.

Samples were immersed in the electrolyte and potential was measured. Potentiodynamic polarization test was started after the initial corrosion potential reached a stable value (after approximately 40 minutes).

The effect of addition of the alloying elements (Cr and Ti) on the polarization curves of Fe40Al alloy are shown in Figure 1, where it can be seen that all the alloys exhibited an active-passive behavior.

Table 2. electrochemical parameters obtained from the polarization curves of FeAl based alloys polarized in Hank solution.

Alloy	E_{corr} (mV)	I_{corr} (mA/cm ²)	E_{pit} (mV)	I_{pit} (mA/m ²)	$E_{\text{pasiv.}}$ (mV)	I_{pasiv} (mA/cm ²)
Fe-40Al	-701.7	4.7×10^{-4}	-384.3	0.0021	-637.8	5.6×10^{-4}
Fe-40Al2.5Ti	-542.2	9.3×10^{-4}	-205.8	0.0045	-480	9.3×10^{-4}
Fe-40Al2.5Cr	-687.3	9.51×10^{-4}	-162.4	0.0154	-622.3	0.0011

Figure 2 and Table 2, show that the most active potential was for the binary Fe40Al (at.%) alloy with $E_{\text{corr}} = -701.7$ mV. Figure 1, also indicates that with the addition of the alloying elements Cr and Ti, the corrosion potential became nobler. The noblest E_{corr} value was for the Fe40Al2.5Ti (at. %) alloy, at approximately -542.2 mV. It is worth nothing that the corrosion potential of the alloys studied in the present work are more active than the corrosion potential of a 316L stainless steel biomaterial which was exposed in Hank solution with E_{corr} close to -210 mV, whose value was previously reported in potentiodynamic polarization test [19].

Also shown in Figure 2 and Table 2, the lowest corrosion current density was for the binary alloy Fe40Al with $I_{\text{corr}} = 4.7 \times 10^{-4}$ mA/cm². The highest value was for the Fe40Al2.5Cr alloy, with $I_{\text{corr}} = 9.5 \times 10^{-4}$ mA/cm², potentially presenting the highest rate of corrosion. The corrosion current density of intermetallic alloys studied in this work, exhibited lower values compared with the corrosion current density of 316 stainless steel ($I_{\text{corr}} = 1.5 \times 10^{-3}$ mA/cm) previously reported [19] using potentiodynamic polarization curves of this steel immersed in Hank's solution. García-Alonso discovered that corrosion rate of a group of annealed Fe₃Al based intermetallic compounds were close than that for 316 L stainless steel in biomimetic human body fluid [10].

Therefore, the FeAl based alloys studied in present work, present a lower corrosion rate than 316 L stainless steel and annealed Fe₃Al-type intermetallic under same condition tests.

Additionally, the binary FeAl alloy exhibited the lowest pitting potential value, E_{pit} , (-384.3 mV), whereas the highest value, was for Fe40Al2.5Cr alloy (-162.4 mV). Previous work [19] reported a pitting potential value of 330 mV in 316 L stainless steel under the same electrochemical test conditions. The data presented here show a greater susceptibility to pitting corrosion for FeAl based intermetallics than for 316 L type stainless steel.

3.3. Linear polarization resistance (LPR) measurements.

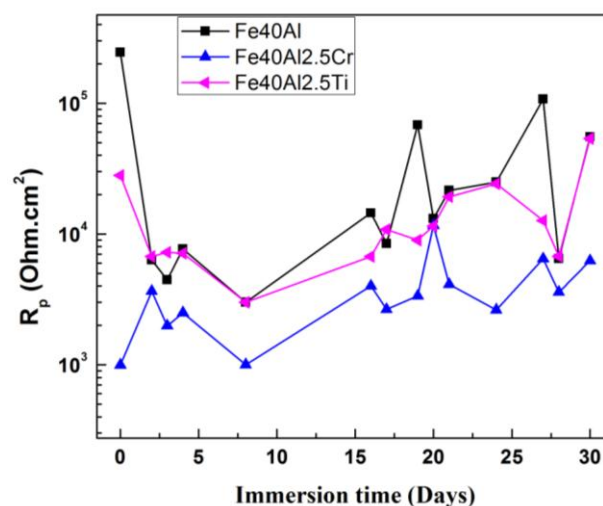


Figure 3. Effect of addition of Cr and Ti in the variation of the linear polarization resistance R_p with time for Fe40Al binary alloy in Hank's solution.

The variation of R_p with time, for the different alloys is displayed in Figure 3, which shows that the R_p value for Fe40Al2.5Cr increased from the beginning of immersion until the second day of the experiment. This behavior may be due to the formation of a passive initial layer of corrosion products. Following two days of immersion, the R_p value of ternary alloys exhibited an erratic variation as the immersion time increased, this behavior can be linked to passivation-repassivation events.

This trend can be explained in terms of the stability of the external corrosion products layer: if this layer is very stable, and it is not detached from the metal surface, the R_p value remains more or less constant, but if this layer is detached and reformed, the R_p value will fluctuate with time.

The value of R_p for the ternary alloys was higher at 30 days of immersion compared with the values of R_p at the start of testing (0 days). However, the value of R_p in the FeAl alloy did not show the same behavior. Such behavior can be due to the formation of passive thick layers constituted by Cr_2O_3 and TiO_2 in the case of Fe40Al2.5Ti and FeAl2.5Cr alloys. Frangini [20] discovered that additions of some metallic elements to NiAl intermetallics such as Cr or Ti improve the Al_2O_3 protectiveness by suppressing detachment of these scales. In addition, the presence of passive layers of iron and aluminum oxides in the Fe-Al intermetallics also contributed to corrosion protection. Therefore, the addition of Cr and Ti to Fe40Al alloy favored the increment of R_p as immersion time elapsed since these elements improve the protectiveness of aluminum oxide layer.

3.4. Electrochemical impedance spectroscopy (EIS) measurements.

EIS data in Nyquist curves obtained for the binary alloy Fe40Al at different exposure times are shown on Figure 4 (a). The Nyquist diagram shows that the curve data at 1, 15 and 30 days of

immersion exhibit two capacitive-like semicircles, a capacitive semicircle at high frequencies and a second semicircle at lower frequencies.

The first semicircle has been associated with the charge-transfer reaction from the alloy into the electrolyte through the electrochemical double layer, while the semicircle observed at low frequency has been linked to the formation of a passive layer, probably Al_2O_3 , Fe_2O_3 , a spinel $FeAl_2O_4$, or corrosion products just as evidenced on polarization curves as shown in Fig. 1.

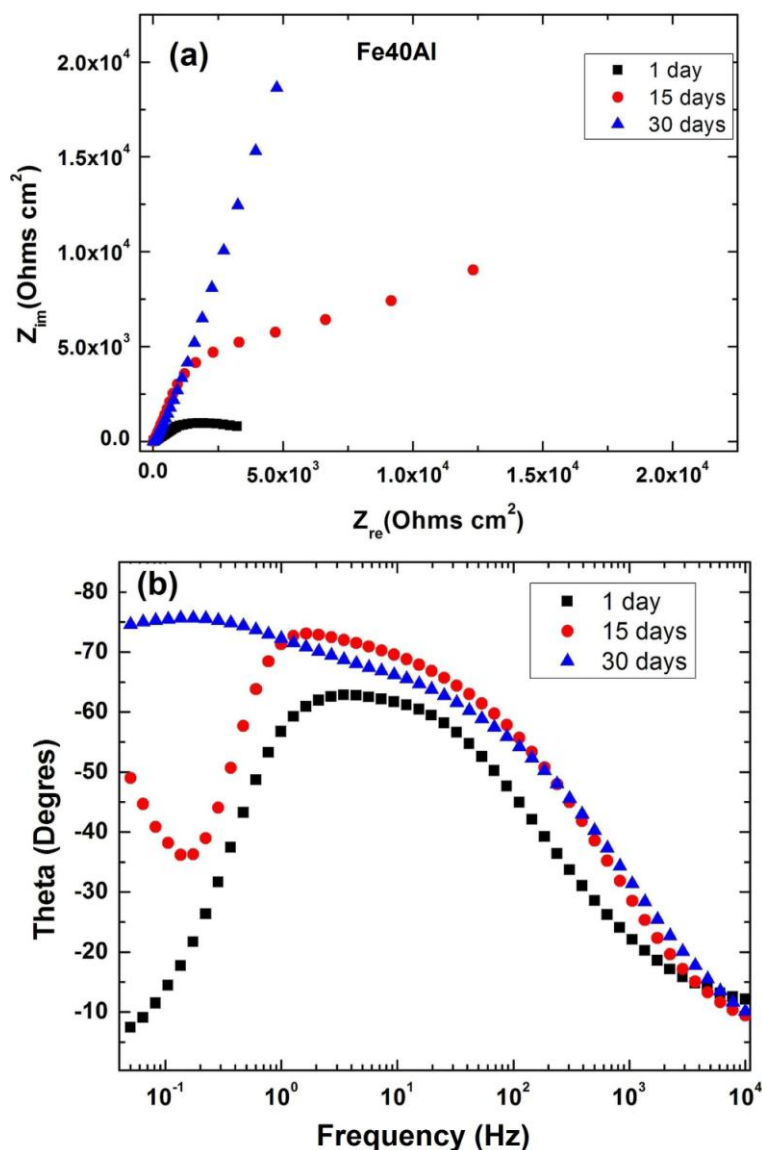


Figure 4. (a) Nyquist curves and (b) Bode phase diagrams at various exposure times for Fe40Al alloy in Hank’s solution at room temperature.

Charge transfer resistance, R_{ct} , is obtained by extrapolating the semicircle located at high frequencies to the diameter of the circle. It was noted that the diameter of the semicircle observed at high frequency corresponding to R_{ct} did not change significantly during the first 15 days of test, but at the end of the period of 30 days of immersion was increased, indicating a decrease in corrosion rate as

time elapsed. Such behavior in turn, may also be associated with the increase of the passive layer's thickness.

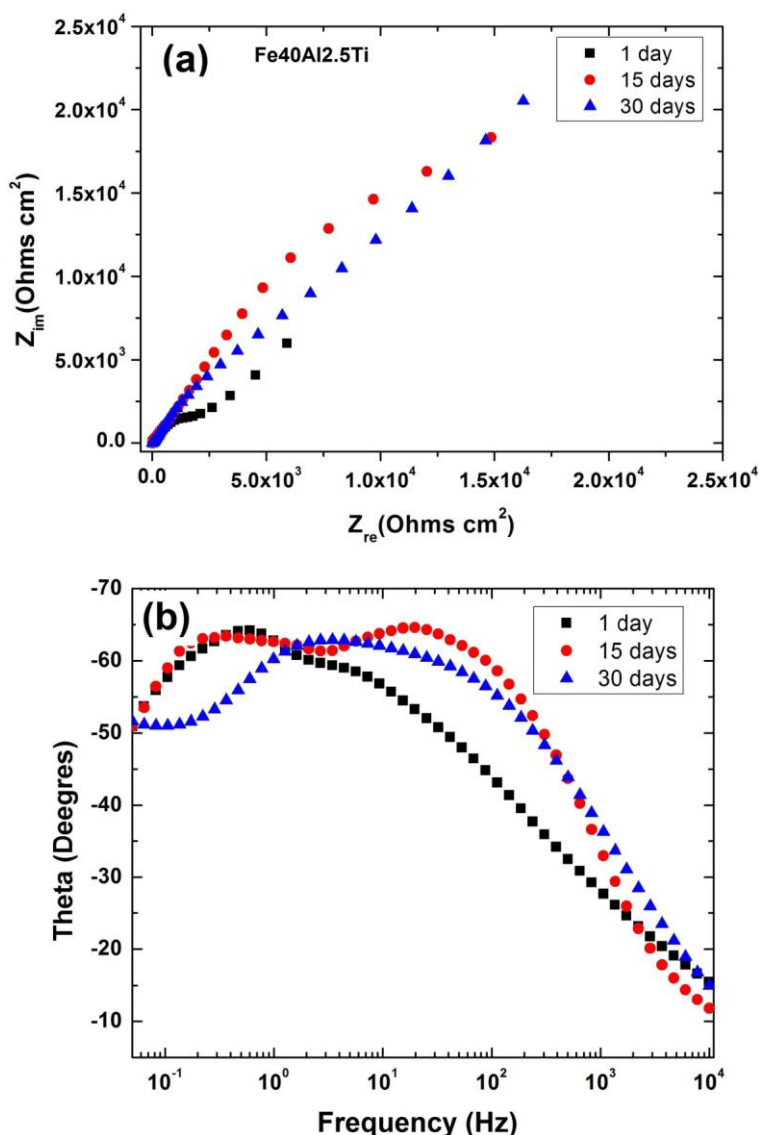


Figure 5. (a) Nyquist curves and (b) Bode phase diagrams at various exposure times for Fe₄₀Al_{2.5}Ti alloy in Hank's solution at room temperature.

On the other hand, Bode-phase diagram displayed on Figure 4 (b) shows two time constants after 14 days of immersion tests, which indicates a highly capacitive behavior, typical of passive alloys, is indicated from medium to low frequencies by phase angles approaching -80° , suggesting that a very stable film is formed on Fe₄₀Al alloy after 14 days of immersion tests in the used electrolyte. EIS data in Nyquist curves were obtained for the binary alloy Fe₄₀Al_{2.5}Ti at different exposure times are shown on Figure 5 (a). The Nyquist diagram shows that the curve data at 1, 15 and 30 days of immersion exhibit two depressed, capacitive-like semicircles, with their centers in the real axis: one at high frequencies and another at intermediate and lower frequency values. The high frequency

semicircle has been associated with the charge-transfer reaction from the alloy into the electrolyte through the electrochemical double layer, while the semicircle observed at low frequency has been linked to the formation of a passive layer, probably Al_2O_3 , Fe_2O_3 , TiO , a spinel FeAl_2O_4 , or corrosion products just as evidenced on polarization curves as shown in figs. 1 and 10.

Charge transfer resistance, R_{ct} , is obtained by extrapolating the semicircle located at high frequencies to the diameter of the circle. It was noted that the diameter of the semicircle observed at high frequency corresponding to R_{ct} increased during the first 15 days of test, but was decreased at the end of the period of 30 days of immersion, indicating an instability in the passive layer after the fifteenth days of immersion tests, (see Table 3).

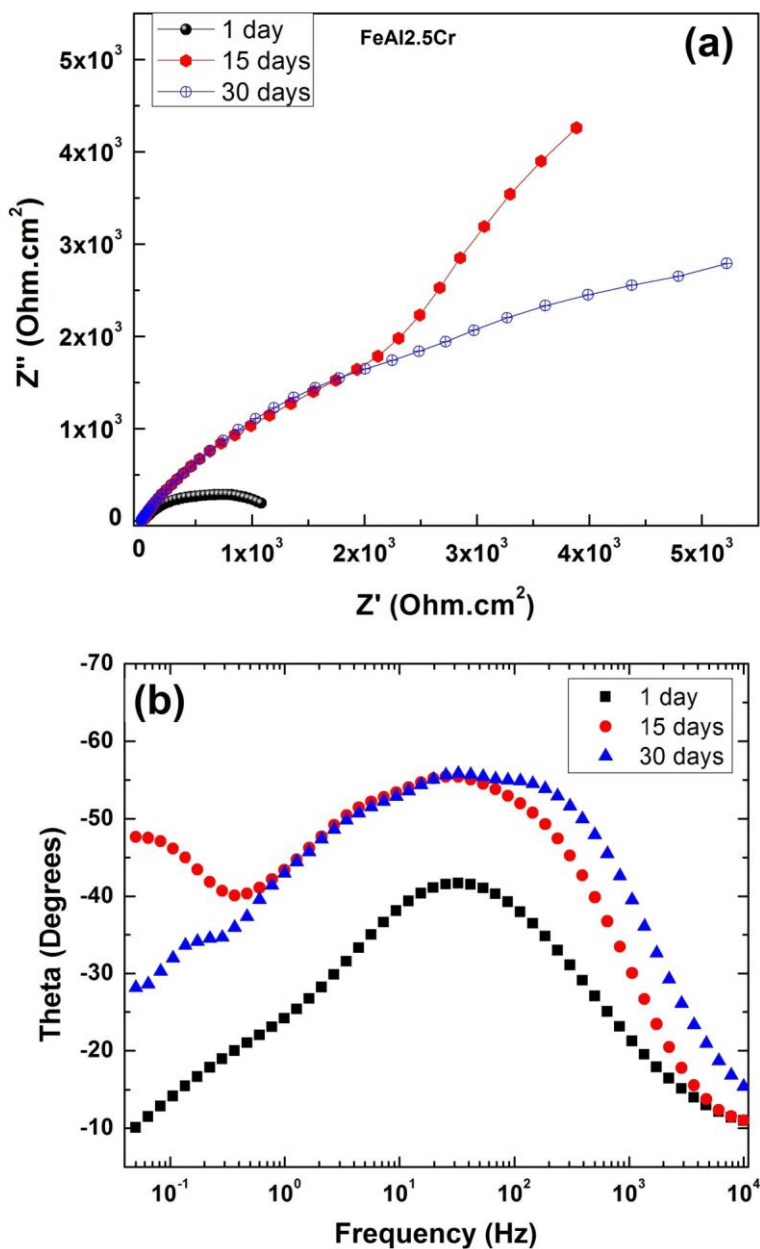


Figure 6. (a) Nyquist curves and (b) Bode phase diagrams at various exposure times for Fe40Al2.5Cr alloy in Hank’s solution at room temperature.

On the other hand, Bode-phase diagram displayed on Figure 5 (b) shows two time constants at all days of immersion tests, which indicates a highly capacitive behavior, typical of passive materials. This capacitive behavior is indicated from medium to low frequencies by phase angles approaching -70° , suggesting that a very stable film is formed on Fe40Al2.5Ti alloy after 14 days of immersion tests in the used electrolyte.

EIS data in Nyquist curves obtained for the ternary alloy Fe40Al2.5Cr at different exposure times are shown on Figure 6 (a). The nyquist diagram shows that the curve data at all days of immersion exhibit two depressed, capacitive-like semicircles, with their centers on the real axis: one at high frequencies and another at intermediate and lower frequency values. The high frequency semicircle has been associated with the charge-transfer reaction from the alloy into the electrolyte through the electrochemical double layer, while the semicircle observed at low frequency has been linked to the formation of a passive layer, probably Al_2O_3 , Fe_2O_3 , CrO , Cr_2O_3 or corrosion products just as evidenced on polarization curves as shown in Figs. 1 and 9.

Charge transfer resistance, R_{ct} , is obtained by extrapolating the semicircle located at high frequencies to the diameter of the circle. It was noted that the diameter of the semicircle observed at high frequency corresponding to R_{ct} increased from first to the fifteenth day of immersion test but after that time decreased slightly towards the second half of the final period of immersion tests, see fig. 6 (a) and table 3, indicating the lower stability of passive film.

The Bode diagram (Fig. 6 b), shows only one time constant on the first day of the immersion test. After this time, the peaks turned coarser, and the frequency interval in which these two time constants were present became wider, indicating the lower stability of the passive film as compared to that present on Fe40Al2.5Ti alloy.

The equivalent electric circuit model used to simulate the EIS data is shown in Fig. 7, where R_s represents the electrolyte or solution resistance, R_{dl} is the double electrochemical layer resistance associated with the charge transfer resistance and C_{dl} its capacitance, R_f is the resistance of the film associated to the participation of the corrosion products and C_f is its capacitance. It is important to note that the equivalent electric circuit model illustrated in Fig. 9 is related to the case when active metals suffer from localized corrosion, as was reported by Zeng et. al. for localized corrosion of metals in molten salts [21].

When a non-ideal frequency response is present, it is commonly accepted practice to use circuit elements in an equivalent circuit. The most widely used is the constant phase element (CPE), which has a non-integer power dependence with frequency.

The impedance of of a CPE is described by the expression:

$$Z_{CPE} = Y^{-1}(j\omega)^{-n}$$

Where Y is a proportional factor, j is $\sqrt{-1}$, ω is the frequency and $-1 < n < 1$ is phase shift. Often a CPE is used in a model instead of a capacitor to compensate for non-homogeneity in the system. Calculated parameters to simulate the EIS data for different intermetallic alloys are shown on Table 3. The resistance of the barrier layer associated to the participation of corrosion products, R_f , is in most of the cases, higher than the resistance of the double electrochemical layer, R_{dl} . This denotes

that corrosion protection is principally given by the inner barrier layer, as also shown in the literature [22, 23].

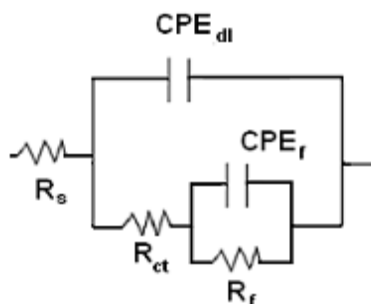


Figure 7. Electric circuit used to simulate the EIS data for tested materials, showing a constant phase element (CPE) circuit equivalency for the capacitive segments.

Table 3. Parameters used to simulate the EIS data for binary and ternary alloys

Time (days)	R_s (Ohm.cm ²)	R_{ct} (Ohm.cm ²)	CPE _{dl} (F)	n_{dl}	CPE _f (F)	n_f	R_f (Ohm.cm ²)
Fe-40Al alloy							
1	3.9×10^1	1.4×10^4	4.8×10^{-5}	0.79	4.2×10^{-5}	0.62	1.5×10^4
15	1.8×10^1	1.1×10^4	4.5×10^{-5}	0.99	5.7×10^{-5}	0.38	9.2×10^4
30	1.8×10^1	4.5×10^5	4.8×10^{-5}	0.83	4.6×10^{-5}	0.89	1.2×10^6
Fe-40Al2.5Ti alloy							
1	2.9×10^1	4.3×10^3	9.3×10^{-5}	0.87	1.1×10^{-4}	0.60	9.9×10^4
15	1.5×10^1	1.3×10^5	8.5×10^{-5}	0.74	8.5×10^{-5}	0.74	5.5×10^4
30	1.3×10^1	4.4×10^4	8×10^{-5}	0.75	7.6×10^{-5}	0.75	4.9×10^5
Fe-40Al2.5Cr alloy							
1	1.9×10^1	9.3×10^2	3.7×10^{-4}	0.48	2.4×10^{-4}	0.48	1×10^3
15	1.8×10^1	9×10^3	1.7×10^{-4}	0.61	2.8×10^{-4}	0.77	2.6×10^4
30	1.3×10^1	7.4×10^3	1.4×10^{-4}	0.63	2.5×10^{-4}	0.81	1.2×10^4

3.5. Microstructural characterization of corroded alloys.

Micrographs of the Fe40Al alloy together with corrosion products on the surface are shown in Fig. 8 (a). Subsection (b) of the same illustration shows the chemical mapping of three elements, Cl

(red), O (green) and Ca (blue). Circular precipitates rich in Ca are observed, which can correspond to a calcium oxide. Figures 8 (b), (c) and (d) indicate a uniform distribution of elements Al, Fe and O (green) on the surface region, which indicate the existence of a protective passive surface layer mainly composed of (Al_2O_3) FeO and Fe_2O_3 , which is located underlying the discontinuous layer of calcium oxide.

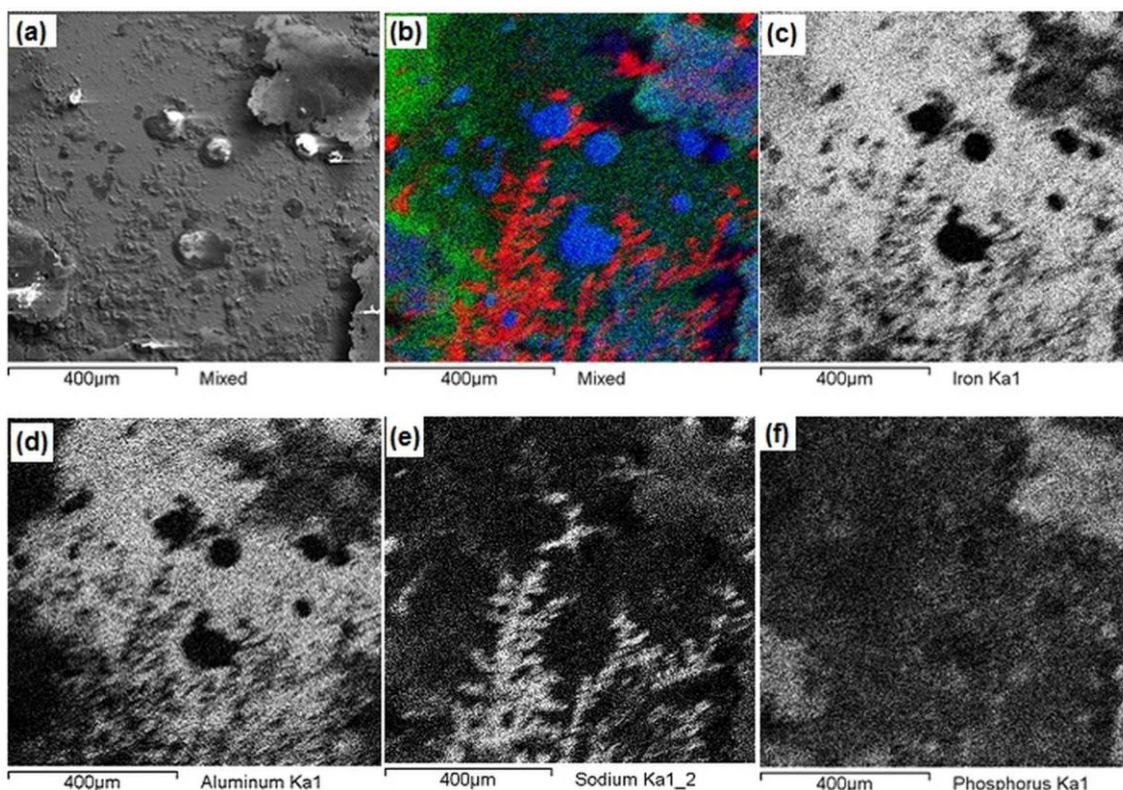


Figure 8. Photomicrographs of FeAl alloy corroded in Hank's solution together with X-Ray mappings of Cl, O, Ca, Fe, Al, Na and P.

Figures 8 (b) and (e) show the chemical mapping of the elements Na and Cl which is related to the precipitation of NaCl on the surface of the intermetallic compound, adopting a branched morphology. Figures 8 (b), (e) and (f) shows the X ray mapping of the elements P, Na and Ca (blue), the regions of coincidence of these three elements likely indicate the presence of calcium phosphate compounds or sodium phosphate.

Figure 9 (a) shows an SEM micrograph where two zones are visible: a smooth region where the matrix elements $Fe_{40}Al_{12.5}Cr$ (% at.) predominate, and a second with greater roughness consisting of a thicker surface layer formed by the corrosion products of Cl, O, Na, P, Ca, and Fe. Figure 9 (b) shows NaCl precipitates over the smooth region where the matrix elements predominate (red particles). This salt can also be observed in the thicker region constituted by the products of corrosion. According to the X-ray mapping shown in Figures 9 b, c, and d, the elements Al, Fe, Cr, and O are distributed not only on the smooth surface of the alloy, but also in the products of corrosion. The

existence of these elements is linked to the passive layer that forms on the surface of these intermetallic compounds. Similarly, in Fig. 9 b, e, and f, the layer consisting of the products of corrosion can also consist of CaO and/or a phosphate.

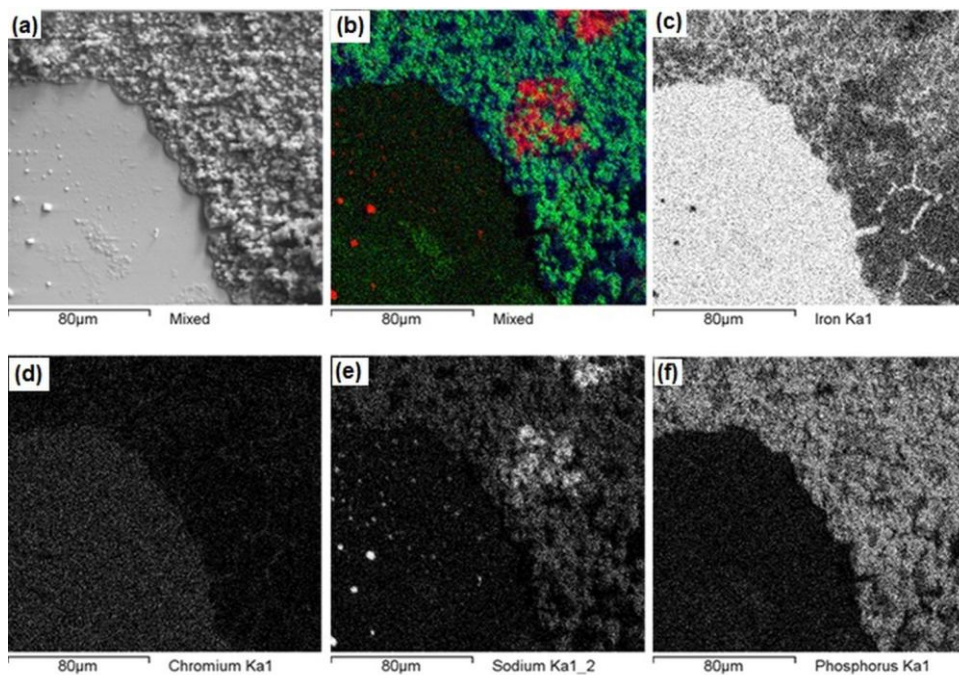


Figure 9. Photomicrographs of FeAl_{2.5}Cr alloy corroded in hank’s solution together with X-Ray mappings of Cl (red), O (green), Ca (blue), Fe, Cr, Na and P.

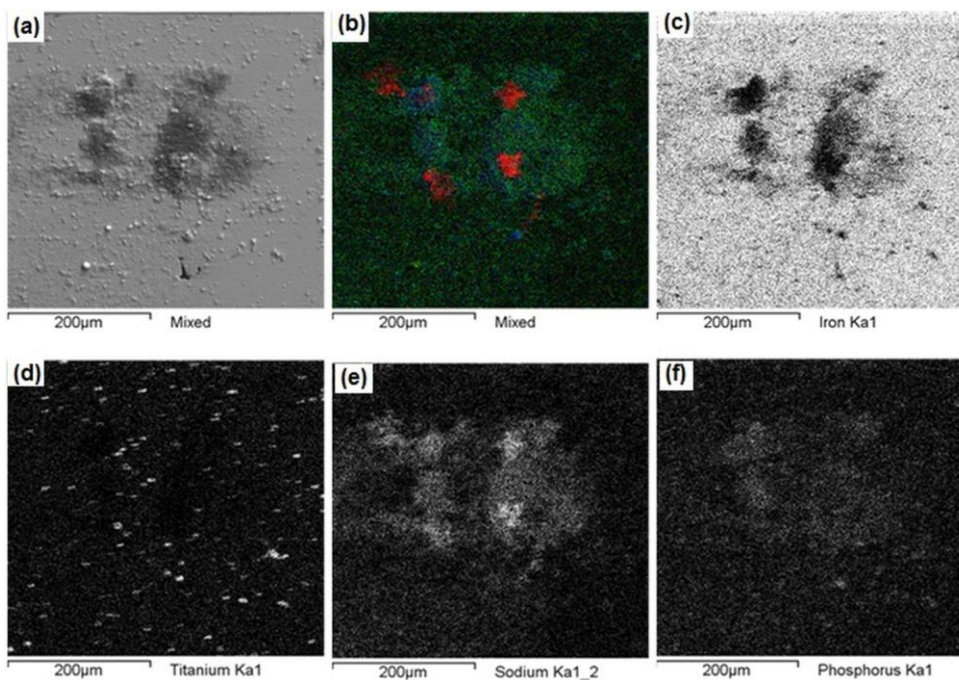


Figure 10. Photomicrographs of FeAl_{2.5}Cr alloy corroded in hank’s solution together with X-Ray mappings of Cl (red), O (green), Ca (blue), Fe, Cr, Na and P.

Figure 10 a) shows the corroded surface of the specimen corresponding to the Fe40Al2.5Ti alloy. The darker stains contain Cl and Na according to the chemical maps shown in Figures 10 b and e), and are due to the presence of NaCl. The darker stains in Figure 10 a) also demonstrate a superficial lack of Al and Fe, while in the same regions there is a reduced quantity of O, Na, Ca, and P observed. This can be linked to the existence of CaO, NaCl, and calcium phosphates. Figure 10 d) shows Ti distributed in clusters throughout the FeAl matrix. According to the chemical maps shown in Figures 10 b and c, a superficial and poorly-defined layer can be observed consisting of Fe, Al, and O, that could be associated with the formation of the Fe₂O₃, Al₂O₃ layer.

4. CONCLUSIONS

The corrosion behavior of FeAl based intermetallic alloys as possible materials to be used in human body environment has been evaluated. Potentiodynamic polarization curves showed that Fe40Al showed the greatest corrosion resistance while the alloy alloyed with 2.5% at. Cr, showed the lowest resistance to corrosion.

The curves of R_p as a function of exposure time showed that all ternary alloys with the exception of the binary alloy showed higher R_p at the end of immersion time in comparison with the initial values of the tests (at 0 days of immersion). Where this behavior may be due to the formation of a thick passive layer formed by the corrosion products besides oxides of Cr, Ti, Fe and Al which formed on the surface of FeAl based alloys.

An equivalent electric circuit was proposed, which includes the presence of a passivating layer (consisting of a combination of oxides of Fe, Al, Cr and Ti) combined with an organic layer, which provides a protection on the surface of intermetallic. The equivalent circuit elements values were determined and it was founded that in most of the cases, the resistance of the barrier layer associated to the participation of corrosion products, R_f , is in most of the cases, higher than the resistance of the double electrochemical layer, R_{dl} . This indicates that corrosion protection is principally given by the inner barrier layer.

Both the binary and ternary alloys studied in the present work had a lower corrosion rate than 316 L stainless steel, according to the potentiodynamic polarization curves.

Similarly, according to the polarization curves, the Fe-Al alloys exhibit greater susceptibility to pitting corrosion than 316 type stainless steel.

We conclude that these Fe-Al alloys show great promise for use in biological applications with their superior corrosion resistance, which may provide a longer and more stable product life cycle for implantable metals materials.

ACKNOWLEDGEMENT

The authors express their gratitude to CONACyT for the financial support granted for the development of this research.

References

1. D. F. Williams, *Proceedings of a Consensus Conference of the European Society for Biomaterials*, Chester, England, 1986.
2. J.S. Hanker, *Science*, 242 4880 (1988) 885.
3. W. Wang, Y. Ouyang, C.K. Poh, *Annals Of The Academy Of Medicine*, 40 (2011) 237.
4. W.R. Wagner, *Annual meeting- society for biomaterials in conjunction with the international biomaterials symposium*, 1999.
5. B. D. Ratner, A. S. Hoffman, F. J. Schoen, J. E. Lemons, *Biomaterials Science: An Introduction to Materials in Medicine*, Second Edition, Elsevier Academic Press, (2004).
6. A. Schroeder, E. Vanderzypen, H. Stich, and F. Sutter, *Int. J. Oral Maxillofacial Surg.* 9 (1981) 15.
7. R. M. Pilliar, and G. C. Weatherly, *CRC Crit. Rev. Biocompatibility*, 1 4 (1984) 371.
8. J. A. Davidson, and F. S. Georgette. *Proc. Soc. Of Manufacturing Engineering*, Itasca, IL (1986).
9. M. Gomez, H. Mancha, A. Salinas, J. L. Rodríguez, J. Escobedo, M. Castro, and M. Mendez, *J. Biomed. Mater. Res.* 34 (1997) 157.
10. M.C. Garcia-Alonso, M.F. Lopez, M.L. Escudero, J.L. Gonzalez-Carrasco and D.G. Morris, *Intermetallics* 7 (1999) 185.
11. M.F. Lopez, M.L. Escudero, E. Vida, A.R. Pierna and F.F. Marzo, *Electrochim. Acta* 42 (1997) 659.
12. M.F. Lopez, A. Gutierrez, M.C. Alonso-Garcia and M.L. Escudero, *J. Mater. Res.* 13(1998) 3144.
13. P.F. Tortorelli, P.S. Bishop, in *Environmental Effects on Advanced Materials, the Minerals, Metals and Materials Society*, Warrendale, P.A., (1991).
14. P. F. Tortorelli, K. Natesan, *Mat. Sci. And Eng.* A258 (1998) 115.
15. V.S. Rao, *Electrochimica. Acta*, 49 (2004) 4533.
16. T.B. Massalski, *Binary Alloy Phase Diagrams*, 1 (1986) 112.
17. D. Li, D. Lin and Y. Liu, *Mat. Sci. and Eng.*, A249 (1998) 206.
18. M. Palm, G. Inden and N. Thomas, *Journal of Phase Equilibria*, 16 3 (1995) 209.
19. I. E. Castañeda, J.G. Gonzalez-Rodriguez, G. Dominguez-Patiño, R. Sandoval-Jabalera, M.A.Neri-Flores, J. G. Chacon-Nava, A. Martinez-Villafañe, *Int. J. Electrochem. Science*, 6 (2011) 404.
20. S. Frangini, A. Masci, *Surf. Coatings Technol.*, 184 (2004) 3.
21. C. L. Zeng, W. Wang, W. T. Wu, *Corrosion Science*, 43 (2001) 787.
22. N.J. Medvedeva, Y.N. Gornostyrev, D.L. Novikov, O.N. Myrasov and A.J. Freeman, *Acta Metall. Mater.* 46 (1998) 3433.
23. Y.L. Zhou, M. Ninomi, T. Akahori, H. Fukui and H. Toda, *Mat. Science. Eng.*, 398A (2005) 28.